January 2004

Center–Edge Asymmetry at Hadron Colliders

E.W. Dvergsnes[a,*], P. Osland[a,†], A.A. Pankov[b,c,‡] and N. Paver[c,§]

[a]Department of Physics and Technology, University of Bergen, N-5007 Bergen, Norway

[b]Pavel Sukhoi Technical University, Gomel 246746, Belarus

[c]University of Trieste and INFN-Sezione di Trieste, 34100 Trieste, Italy

Abstract

We investigate the possibility of using the center–edge asymmetry to distinguish graviton exchange from other new physics effects at hadron colliders. Specifically, we study lepton-pair production within the ADD and RS scenarios. At the Tevatron, the graviton-Z interference is the most important contribution to the center–edge asymmetry, whereas at the LHC, the dominant contribution comes from gluon fusion via graviton exchange, which has no analogue at e^+e^- colliders. We find that spin-2 and spin-1 exchange can be distinguished up to an ADD cut-off scale, M_H, of about 5 TeV, at the 95% CL. In the RS scenario, spin-2 resonances can be identified in most of the favored parameter space.

*erik.dvergsnes@fi.uib.no

†per.osland@fi.uib.no

‡pankov@gstu.gomel.by

§nello.paver@ts.infn.it

1 Introduction

There exists a variety of proposals of what may come beyond the Standard Model (SM), many different scenarios introduce new fundamental particles and forces at very high mass scales. Some of these different proposals are: composite models of quarks and leptons [1, 2]; exchanges of heavy Z' [3, 4] and (scalar and vector) leptoquarks [5]; R-parity breaking sneutrino exchange [6, 7]; anomalous gauge boson couplings [8]; Kaluza–Klein (KK) graviton exchange, exchange of gauge boson KK towers or string excitations, *etc.* [9–16]. There is a hope that new physics (NP) effects will be observed either directly, as in the case of new particle production, e.g., Z' and W' vector bosons, SUSY or Kaluza-Klein (KK) resonances, or indirectly through deviations, from the SM predictions, of observables such as cross sections and asymmetries.

Over the last years, intensive studies have been carried out, of how different scenarios involving extra dimensions [14–18] would manifest themselves at high energy colliders such as the Tevatron, the Large Hadron Collider (LHC) and an e^+e^- Linear Collider (LC) [9–16]. We shall consider the possibility of distinguishing such effects of extra dimensions from other NP scenarios at hadron colliders, focusing on two specific models involving extra dimensions, namely the Arkani-Hamed–Dimopoulos–Dvali (ADD) [14] and Randall–Sundrum (RS) [15] scenarios with emphasis on the lepton pair production process. These models lead to very different phenomenologies and collider signatures.

The large extra dimension scenario (ADD) predicts the emission and exchange of KK towers of gravitons. The effect of the graviton towers can be described through a set of dimension-8 operators characterized by a large cut-off scale, M_H [9]. The distortion of the differential Drell-Yan cross section at large values of the dilepton invariant mass through these dimension-8 operators can probe such high mass scales in a manner similar to searches for contact interactions in composite models. The shape of the invariant mass distribution will tell us that the underlying physics arises from dimension-8 operators, while the angular distribution of the leptons at large dilepton invariant masses would have the shape expected from the exchange of a spin-2 object, confirming the gravitational origin of the effect.

The phenomenology of the RS model with warped extra dimensions is very different from the ADD model in two aspects: (i) the spectrum of the graviton KK states are discrete and unevenly spaced while it is uniform, evenly spaced, and effectively a continuous spectrum in the ADD model, and (ii) each resonance in the RS model has a coupling strength of 1/TeV while in the ADD model only the collective strength of all graviton KK states gives a coupling strength 1/TeV. The RS model predicts TeV-scale graviton resonances which might be produced in many channels, including the dilepton channel. The spin-2 nature of the graviton resonance can be determined from the distinct shape of the angular distribution of the final state leptons in Drell-Yan production at the Tevatron and LHC.

Many different NP scenarios may lead to the same or very similar experimental signatures. Therefore, searching for effects of extra dimensions can be jeopardized by the misidentification of their signal with other possible sources of new phenomena. Thus, it is

important to study how to differentiate the corresponding signals.

One can develop techniques which will help dividing models into distinct subclasses. In this paper we shall discuss a technique that makes use of the specific modifications in angular distributions induced by spin-2 exchanges. This method is based on the center-edge asymmetry $A_{\rm CE}$ [11, 19], an integrated observable which offers a way to uniquely identify KK graviton exchange (or any other spin-2 exchange). In a situation with limited statistics, this may represent an advantage over a fit to the angular distribution.

In Sec. 2 we define a hadron collider version of the center–edge asymmetry, and give the cross sections relevant for lepton production. Thereafter, in Sec. 3, we study the effects of introducing angular cuts related to the detector geometries. In Sec. 4 we then discuss how the center–edge asymmetry can be used to identify spin-2 exchange at both the LHC and the Tevatron. Finally, in Sec. 5 we summarize our results.

2 The center–edge asymmetry $A_{\rm CE}$

At hadron colliders, lepton pairs can in the SM be produced at tree-level via the following sub-process

$$q\bar{q} \to \gamma, Z \to l^+l^-, \tag{2.1}$$

where we shall use $l = e, \mu$. If gravity can propagate in extra dimensions, the possibility of KK graviton exchange opens up two tree-level channels at hadron colliders in addition to the SM channels, namely

$$\begin{aligned} q\bar{q} &\to G \to l^+l^-, \\ gg &\to G \to l^+l^-, \end{aligned} \tag{2.2}$$

where G represents the gravitons of the KK tower. At the LHC, the gluon-fusion channel can give an important contribution, since it has a different angular distribution arising from the difference between the gluon-graviton and quark-graviton couplings, combined with the high gluon luminosities.

Consider a lepton pair of invariant mass M at rapidity y (of the parton c.m. frame) and with $z = \cos\theta_{\rm cm}$, where $\theta_{\rm cm}$ is the angle, in the c.m. frame of the two leptons, between the lepton (l^-) and the proton P_1. The inclusive differential cross section for producing such a pair, can at the LHC proton-proton collider be expressed as

$$\begin{aligned} \frac{d\sigma_{q\bar{q}}}{dM\,dy\,dz} &= K\frac{2M}{s}\sum_q \Bigg\{ [f_{q|P_1}(\xi_1,M) f_{\bar{q}|P_2}(\xi_2,M) + f_{\bar{q}|P_1}(\xi_1,M) f_{q|P_2}(\xi_2,M)] \frac{d\hat{\sigma}^{\rm even}_{q\bar{q}}}{dz} \\ &\qquad + [f_{q|P_1}(\xi_1,M) f_{\bar{q}|P_2}(\xi_2,M) - f_{\bar{q}|P_1}(\xi_1,M) f_{q|P_2}(\xi_2,M)] \frac{d\hat{\sigma}^{\rm odd}_{q\bar{q}}}{dz} \Bigg\}, \\ \frac{d\sigma_{gg}}{dM\,dy\,dz} &= K\frac{2M}{s}\, f_{g|P_1}(\xi_1,M) f_{g|P_2}(\xi_2,M) \frac{d\hat{\sigma}_{gg}}{dz}. \end{aligned} \tag{2.3}$$

Here, $d\hat{\sigma}^{\rm even}_{q\bar{q}}/dz$ and $d\hat{\sigma}^{\rm odd}_{q\bar{q}}/dz$ are the even and odd parts (under $z \leftrightarrow -z$) of the partonic differential cross section $d\hat{\sigma}_{q\bar{q}}/dz$, and the minus sign in the odd term allows us to interpret

the angle in the parton cross section as being relative to the quark momentum (rather than P_1). Furthermore, K is a factor accounting for higher order QCD corrections (we take $K = 1.3$, which is a typical value), $f_{j|P_i}(\xi_i, M)$ are parton distribution functions in the proton P_i, and the ξ_i are fractional parton momenta

$$\xi_1 = \frac{M}{\sqrt{s}} e^{y}, \qquad \xi_2 = \frac{M}{\sqrt{s}} e^{-y}. \tag{2.4}$$

We also made use of the relation $d\xi_1\, d\xi_2 = dM(2M/s)dy$ and have $M^2 = \xi_1 \xi_2 s$, with s the pp c.m. energy squared.

At the Tevatron, taking into account that one beam consists of antiprotons, the following substitution must be made in (2.3):

$$P_1 \to P, \quad P_2 \to \bar{P}. \tag{2.5}$$

The center–edge and total cross sections can at the parton level be defined like for initial-state electrons and positrons [11, 19]:

$$\hat{\sigma}_{\mathrm{CE}} \equiv \left[\int_{-z^*}^{z^*} - \left(\int_{-1}^{-z^*} + \int_{z^*}^{1} \right) \right] \frac{d\hat{\sigma}}{dz}\, dz, \quad \hat{\sigma} \equiv \int_{-1}^{1} \frac{d\hat{\sigma}}{dz}\, dz. \tag{2.6}$$

These will play a central role in the center–edge asymmetry at the hadron level. At this point, $0 < z^* < 1$ is just an arbitrary parameter which defines the border between the "center" and the "edge" regions.

At hadron colliders, the center–edge asymmetry can for a given dilepton invariant mass M be defined as

$$A_{\mathrm{CE}}(M) = \frac{d\sigma_{\mathrm{CE}}/dM}{d\sigma/dM}, \tag{2.7}$$

where we obtain $d\sigma_{\mathrm{CE}}/dM$ and $d\sigma/dM$ from (2.3) by integrating over z according to Eq. (2.6) and over rapidity between $-Y$ and Y, with $Y = \log(\sqrt{s}/M)$. Furthermore [see Eq. (2.3)],

$$\frac{d\sigma}{dM} = \frac{d\sigma_{q\bar{q}}}{dM} + \frac{d\sigma_{gg}}{dM}. \tag{2.8}$$

We note that terms in the parton cross sections that are odd in z do not contribute to A_{CE}; and that

$$\left.\frac{d\sigma_{\mathrm{CE}}}{dM}\right|_{z^*=0} = -\frac{d\sigma}{dM}, \qquad \left.\frac{d\sigma_{\mathrm{CE}}}{dM}\right|_{z^*=1} = \frac{d\sigma}{dM}. \tag{2.9}$$

Conversely, the odd terms of the partonic cross section determine the familiar forward-backward asymmetry A_{FB}:

$$\left(\frac{d\sigma}{dM}\right) A_{\mathrm{FB}}(M) = \left(\int_0^Y \mp \int_{-Y}^0 \right) dy \left(\int_0^1 - \int_{-1}^0 \right) dz\, \frac{d\sigma}{dM\, dy\, dz}, \tag{2.10}$$

where the two signs in the integration over y refer to the proton-proton and proton-antiproton cases, respectively. Note that on the right-hand side of Eq. (2.10) the gluon-gluon channel will not contribute, as it is symmetric in z.

In order to develop some intuition for the different contributions to the cross section, and to the asymmetry $A_{\rm CE}(M)$, we shall first study the ideal case where no angular cuts have been imposed. The modifications caused by quasi-realistic cuts will be discussed in Sec. 3.

2.1 $A_{\rm CE}$ in the ADD Scenario

Let us now consider the ADD scenario [14], where gravity is allowed to propagate in two or more compactified, but still large, extra dimensions. This gives rise to a tower of (massive) KK gravitons with tiny mass splittings. In the Hewett approach [9, 20], the summation over KK states (of mass $m_{\vec{n}}$) is performed by the following substitution:

$$\sum_{\vec{n}=1}^{\infty} \frac{G_{\rm N}}{M^2 - m_{\vec{n}}^2} \to \frac{-\lambda}{\pi\, M_H^4}, \tag{2.11}$$

where λ is a sign factor, and $G_{\rm N}$ is Newton's constant. This approach takes into account the fact that the ultraviolet behavior of the scenario is unknown (for a recent discussion, see [21]). In particular, there is no dependence on the number of extra dimensions.

We then have the following parton differential cross sections [22], where double superscripts refer to interference between the respective amplitudes (with z the cosine of the quark-lepton angle in the dilepton c.m. frame, and averaged over quark and gluon colors):

$$\begin{aligned}
&\frac{d\hat\sigma_{gg}^{G}}{dz} = \frac{\lambda^2 M^6}{64\pi M_H^8}(1-z^4), && \frac{d\hat\sigma_{q\bar q}^{G}}{dz} = \frac{\lambda^2 M^6}{96\pi M_H^8}(1-3z^2+4z^4),\\
&\frac{d\hat\sigma_{q\bar q}^{G\gamma}}{dz} = -\frac{\lambda\alpha Q_q Q_e M^2}{6M_H^4} z^3, && \frac{d\hat\sigma_{q\bar q}^{GZ}}{dz} = \frac{\lambda\alpha M^2}{12 M_H^4}[a_q a_e(1-3z^2) - 2v_q v_e z^3]{\rm Re}\,\chi,\\
&\frac{d\hat\sigma_{q\bar q}^{\rm SM}}{dz} = \frac{\pi\alpha^2}{6M^2}[S_q\,(1+z^2) + 2A_q\, z].
\end{aligned} \tag{2.12}$$

Here, fermion masses are neglected, and we define

$$\begin{aligned}
S_q &\equiv Q_q^2 Q_e^2 + 2Q_q Q_e v_q v_e\,{\rm Re}\,\chi + (v_q^2+a_q^2)(v_e^2+a_e^2)\,|\chi|^2,\\
A_q &\equiv 2Q_q Q_e a_q a_e {\rm Re}\,\chi + 4 v_q a_q v_e a_e |\chi|^2.
\end{aligned} \tag{2.13}$$

We use a convention where $a_f = T_f$, $v_f = T_f - 2Q_f \sin^2\theta_W$ and the Z propagator is represented by

$$\chi = \frac{1}{\sin^2(2\theta_W)}\,\frac{M^2}{M^2 - m_Z^2 + i m_Z \Gamma_Z}. \tag{2.14}$$

From Eqs. (2.6) and (2.12), we obtain the following parton level center–edge cross sections

$$\hat\sigma_{gg,{\rm CE}}^{G} = \frac{\lambda^2 M^6}{40\pi M_H^8}[\tfrac{1}{2} z^*(5 - z^{*\,4}) - 1], \qquad \hat\sigma_{q\bar q,{\rm CE}}^{G} = \frac{\lambda^2 M^6}{60\pi M_H^8}[2 z^{*\,5} + \tfrac{5}{2} z^*(1 - z^{*\,2}) - 1],$$

$$\hat{\sigma}^{G\gamma}_{q\bar{q},\mathrm{CE}} = 0, \qquad \hat{\sigma}^{GZ}_{q\bar{q},\mathrm{CE}} = \frac{\lambda\alpha a_q a_e M^2}{3M_H^4}\,\mathrm{Re}\,\chi[z^*(1-z^{*\,2})],$$
$$\hat{\sigma}^{\mathrm{SM}}_{q\bar{q},\mathrm{CE}} = \frac{4\pi\alpha^2}{9M^2}\,S_q\,[\tfrac{1}{2}z^*(z^{*\,2}+3)-1]. \tag{2.15}$$

Note that, in contrast to the integrated cross section, where both $\hat{\sigma}^{G\gamma}_{q\bar{q}}$ and $\hat{\sigma}^{GZ}_{q\bar{q}}$ vanish, the interference between graviton and Z exchange may play an important role in enhancing the sensitivity to the graviton exchange. Actually, one should observe from Eqs. (2.12) and (2.6) that such interference is suppressed, for $M/M_H < 1$, by a factor $(M/M_H)^4$ relative to the SM, while all "pure" graviton exchange contributions are suppressed by the more severe factor $(M/M_H)^8$. Therefore, in particular, the gluon-gluon channel is expected to give a significant contribution only at the LHC collider thanks to the large gluon-gluon luminosities available there.

For the SM contribution to the center–edge asymmetry, we see that the convolution integrals, depending on the parton distribution functions, cancel, and the result is

$$A^{\mathrm{SM}}_{\mathrm{CE}} = \tfrac{1}{2}\,z^*(z^{*2}+3)-1, \tag{2.16}$$

which is independent of M and identical to the result for e^+e^- colliders [11]. Hence, in the case of no cuts, there is a unique value, z^*_0, of z^* for which $A^{\mathrm{SM}}_{\mathrm{CE}}$ vanishes [23]:

$$z^*_0 = (\sqrt{2}+1)^{1/3} - (\sqrt{2}-1)^{1/3} \simeq 0.596, \tag{2.17}$$

corresponding to $\theta_{\mathrm{cm}} = 53.4^\circ$.

The structure of the differential SM cross section of Eq. (2.12) is particularly interesting in that it is equally valid for a wide variety of NP models: composite-like contact interactions, Z' models, TeV-scale gauge bosons, *etc.* Conventional four-fermion contact-interaction effects of the vector–vector kind would yield the same center–edge asymmetry as the SM. If however KK graviton exchange is possible, the tensor couplings would yield a different angular distribution, hence a different dependence of A_{CE} on z^*. In particular, the center–edge asymmetry would not vanish for the same choice of $z^* = z^*_0$ and, moreover, would show a non-trivial dependence on M. Thus, a value for A_{CE} different from $A^{\mathrm{SM}}_{\mathrm{CE}}$ would indicate non-vector exchange NP.

The other important difference from the spin-1 exchange originating from $q\bar{q}$ annihilation is that the graviton also couples to gluons, and therefore, it has the additional gg initial state available, see Eq. (2.12). As a result of including graviton exchange, the center–edge asymmetry is no longer the simple function of z^* in Eq. (2.16).

2.1.1 Parton-level asymmetry

We start the quantitative discussion of the A_{CE} asymmetry by considering a simple, limiting case which illustrates, at the parton level, the M-behavior of the gg vs. $q\bar{q}$ subprocesses and the corresponding interference with the SM. In Fig. 1 we show the 'parton-level' quantity

$$\widehat{A}_{\mathrm{CE}} \equiv \frac{\hat{\sigma}_{\mathrm{CE}}}{\hat{\sigma}}, \tag{2.18}$$

where

$$\hat{\sigma}_{\rm CE} = \hat{\sigma}^G_{u\bar{u},{\rm CE}} + \hat{\sigma}^G_{gg,{\rm CE}} + \hat{\sigma}^{GZ}_{u\bar{u},{\rm CE}}, \tag{2.19}$$

and

$$\hat{\sigma} = \hat{\sigma}^G_{u\bar{u}} + \hat{\sigma}^G_{gg} + \hat{\sigma}^{\rm SM}_{u\bar{u}}. \tag{2.20}$$

Thus, in this example, we take the 'protons' to consist of only u quarks, u antiquarks and gluons. In a collision among such 'protons', we also require the probability of finding a $u\bar{u}$ pair to be equal to the probability of finding a gg pair (the respective convolution integrals are set equal to unity), independent of the invariant mass M. In this limit, the mass dependence arises solely from the parton-level cross sections. Furthermore, we consider $z^* = z_0^* \simeq 0.596$, such that $\hat{\sigma}^{\rm SM}_{u\bar{u},{\rm CE}} = 0$. We note that in the limit $M \gg M_Z$, the contributions to $\widehat{A}_{\rm CE}$ given in Fig. 1 are of the form $f(M/M_H)$.

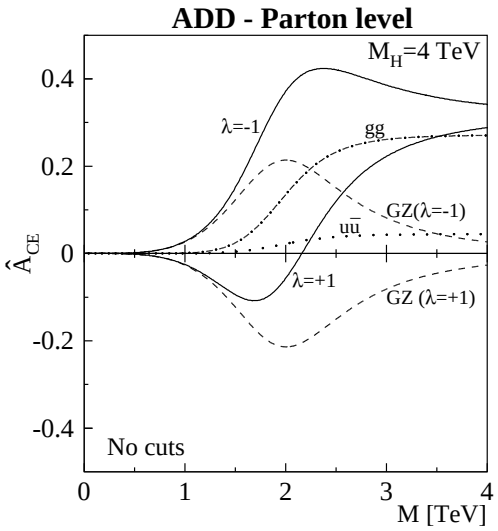

Figure 1: Different contributions to $\widehat{A}_{\rm CE}$ as a function of M in the ADD scenario, for $M_H = 4$ TeV. A simplified parton-level situation is considered, see text. Solid curves: total (parton-level) center–edge asymmetry ($\lambda = \pm 1$), dash-dotted: gg contribution, dotted: $u\bar{u}$ with graviton exchange, dashed: $u\bar{u}$ interference between graviton and Z (labeled GZ).

Since $\hat{\sigma}^{GZ}_{qq,{\rm CE}} \propto a_e a_q$, a cancellation would occur if both d- and u-quarks ($a_d = -a_u$) were considered with equal weight. This cancellation is only partial when differences in parton distributions are accounted for.

For $z^* = z_0^*$ as suggested by Eq. (2.17), and considering the limits of pure glue–glue and pure $q\bar{q}$, we find:

$$\widehat{A}^G_{gg,{\rm CE}} = \frac{\hat{\sigma}^G_{gg,{\rm CE}}}{\hat{\sigma}^G_{gg}} = \tfrac{1}{2}\, z_0^*(5 - z_0^{*\,4}) - 1 \simeq 0.453,$$

$$\widehat{A}^G_{q\bar{q},\mathrm{CE}} = \frac{\hat{\sigma}^G_{q\bar{q},\mathrm{CE}}}{\hat{\sigma}^G_{q\bar{q}}} = 2z_0^{*\,5} + \tfrac{5}{2}\, z_0^*(1 - z_0^{*\,2}) - 1 \simeq 0.111, \tag{2.21}$$

which shows that gluon-fusion events are more "centered" than quark-antiquark annihilation events with graviton exchange. Furthermore, since both quantities in (2.21) are positive, pure graviton events are in general more centered than SM events.

From the cross section formulas (2.15) [see also (2.9)] we see that $\hat{\sigma}^G_{gg} = (3/2)\hat{\sigma}^G_{u\bar{u}}$. At very large M, the SM result, and therefore also the interference, will be negligible. In this case, $\hat{\sigma}^G_{gg}$ and $\hat{\sigma}^G_{u\bar{u}}$ will contribute 60% and 40% to the cross section. Therefore, for large M, using the values of Eq. (2.21), we find that $\widehat{A}_{\mathrm{CE}} \to 0.6 \times 0.453 + 0.4 \times 0.111 = 0.314$, in agreement with Fig. 1. This limit is also applicable at the peak of an RS-graviton resonance (where the interference vanishes). However, as we shall see below, when parton distributions are included, the simple relation 3:2 between the cross sections for gluon fusion and quark-antiquark annihilation with graviton exchange is no longer valid.

2.1.2 Including parton distributions

When parton distributions are included, the picture changes, since the relative probabilities of finding a gg pair and a $q\bar{q}$ pair of invariant mass M will depend on M, as well as on the collision energy, and whether one considers the Tevatron ($p\bar{p}$) or the LHC (pp). In Fig. 2 we show A_{CE} (for $z_0^* \simeq 0.596$) in the ADD model as a function of invariant dilepton mass, M. In the left panel we consider $p\bar{p}$ collisions, where we have chosen the cut-off $M_H = 1.4$ TeV, $\lambda = \pm 1$ and $\sqrt{s} = 1.96$ TeV (Tevatron), whereas in the right panel pp collisions are considered, with $M_H = 4$ TeV, $\lambda = \pm 1$ and $\sqrt{s} = 14$ TeV (LHC). In both plots, the SM contribution, $A^{\mathrm{SM}}_{\mathrm{CE}}$, to the center–edge asymmetry vanishes. To compute cross sections we use the CTEQ6 parton distributions [24].

At the Tevatron, it is the graviton-Z interference term which is dominant, whereas the gluon-fusion channel is almost negligible at this energy. We note that the interference between the graviton and Z amplitude has opposite sign compared to that which occurs in the process $e^+e^- \to l^+l^-$ [11]. This is because there is a difference in sign between the axial vector couplings a_u and a_ℓ, $u\bar{u} \to l^+l^-$ being the most important initial-state $q\bar{q}$ channel. From Eq. (2.15) it is obvious that only the graviton-Z interference term is affected by the choice of λ.

The situation is quite different at a pp collider like the LHC. Here we see that the contribution from gluon fusion (dash-dotted) actually is the most important one. As a result, A_{CE} becomes positive at large M, independent of the sign of λ.

2.2 A_{CE} in the RS Scenario

Another scenario involving extra dimensions, is the RS scenario [15]. Here we shall consider the simplest version of this scenario, with only one extra dimension. The main difference from the ADD scenario is that there will be narrow graviton resonances with masses of the order of TeV, with couplings comparable to weak couplings.

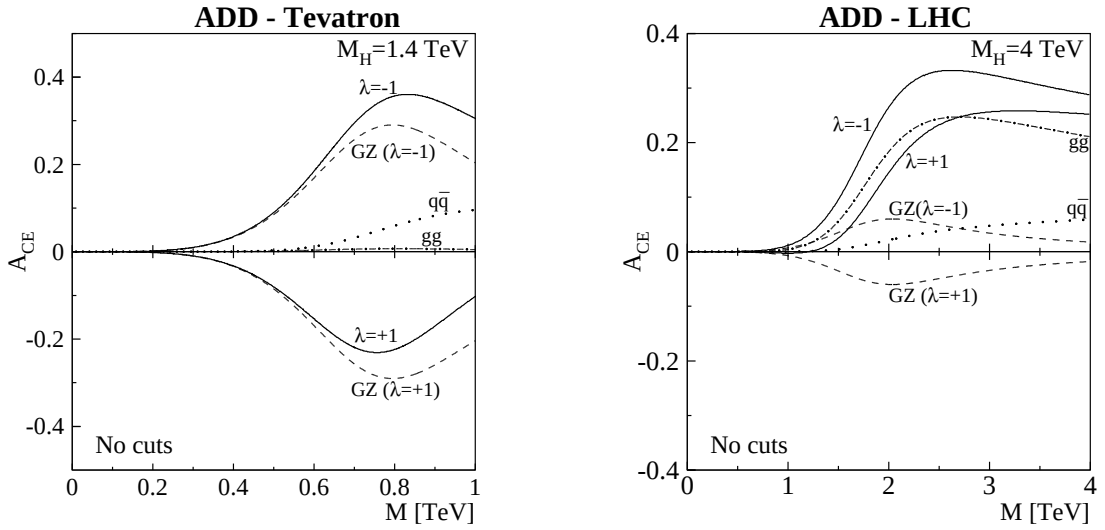

Figure 2: Different contributions to $A_{\rm CE}(M)$ in the ADD scenario. Left panel: Tevatron, $\sqrt{s} = 1.96$ TeV; Right panel: LHC, $\sqrt{s} = 14$ TeV. Solid curves: total center–edge asymmetry ($\lambda = \pm 1$), dash-dotted: gg contribution, dotted: $q\bar{q}$ with graviton exchange, dashed: $q\bar{q}$ interference between graviton and Z (labeled GZ).

In the RS scenario, the spacing between KK resonances can give some hints to the underlying physics. However, it is conceivable that the second resonance would be outside the accessible range of the experiment, such that only the first one would be discovered. It would then be of great interest to determine whether it is a graviton resonance or something less exotic, like a Z' with vector couplings.

This model has two independent parameters, which we take to be $k/\bar{M}_{\rm Pl}$ and m_1, where k is a constant of $\mathcal{O}(\bar{M}_{\rm Pl})$ ($k/\bar{M}_{\rm Pl}$ is in the range 0.01 to 0.1 [10]), and m_1 is the mass of the first graviton resonance. The summation over KK states is performed without using the substitution in Eq. (2.11), but instead modifying in the left-hand side the graviton coupling to matter

$$G_{\rm N} \to \frac{x_1^2}{8\pi m_1^2} \left(\frac{k}{\bar{M}_{\rm Pl}} \right)^2 , \tag{2.22}$$

while keeping the sum over propagators. Here, $x_1 = 3.8317$ is the first root of the Bessel function $J_1(x_n) = 0$ [15, 10].

The deviations of $A_{\rm CE}$ from the SM value (which is zero for $z^* = z_0^*$ as defined in (2.17), still without introducing any cuts) are localized in the invariant mass of the lepton pair around the resonance mass, as is illustrated in Fig. 3 for $k/\bar{M}_{\rm Pl} = 0.05$ and $m_1 = 500$ GeV ($m_1 = 2.5$ TeV) at the Tevatron (LHC). For this choice of parameters, it is unlikely that the second resonance will be discovered. We have used the definition of $A_{\rm CE}$ given in Eq. (2.7).

The graviton-Z interference term vanishes, and thus changes sign, at the resonance

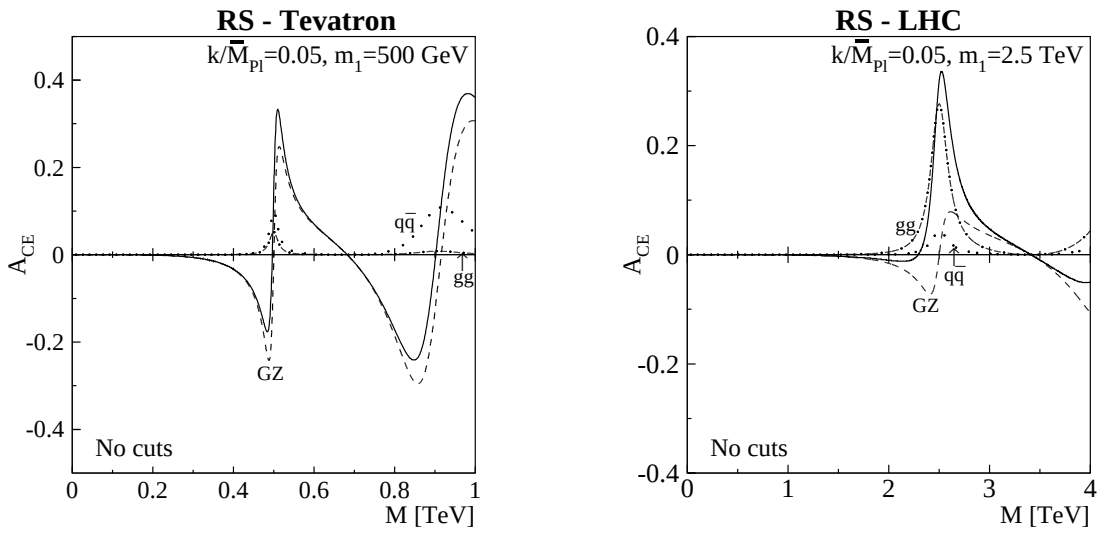

Figure 3: Different contributions to $A_{\rm CE}(M)$ in the RS scenario, with $k/\bar{M}_{\rm Pl} = 0.05$. Left panel: Tevatron, $\sqrt{s} = 1.96$ TeV, $m_1 = 0.5$ TeV; Right panel: LHC, $\sqrt{s} = 14$ TeV, $m_1 = 2.5$ TeV. Solid curves: total center–edge asymmetry, dash-dotted: gg contribution, dotted: $q\bar{q}$ with graviton exchange, dashed: $q\bar{q}$ interference between graviton and Z.

$M = m_1$. At "low" energies, this interference gives the dominant contribution to $A_{\rm CE}$ (see left panel of Fig. 3). This implies that if one integrates over some region in M around the resonance, there will be a strong cancellation. In fact, the contribution from graviton-SM interference almost vanishes when integrated symmetrically around the resonance in the RS scenario, reducing the search reach for gravitons in the RS model at the Tevatron, when using the center–edge asymmetry. This is not the situation for the high energy attained at LHC, dominated in practice by the gg process with graviton exchange, see Fig. 3.

3 Introducing cuts

We next introduce angular cuts, in order to account for the fact that detectors have a region of reduced or no efficiency close to the beam direction. Thus, $d\sigma/dM$ and $d\sigma_{\rm CE}/dM$ of Eq. (2.7) are replaced by

$$\begin{aligned}
\frac{d\sigma}{dM} &= \int_{-y_{\rm max}}^{y_{\rm max}} dy \int_{-z_{\rm cut}}^{z_{\rm cut}} \frac{d\sigma}{dM\, dy\, dz} dz, \\
\frac{d\sigma_{\rm CE}}{dM} &= \int_{-y_{\rm max}}^{y_{\rm max}} dy \left[\int_{-z^*}^{z^*} - \left(\int_{-z_{\rm cut}}^{-z^*} + \int_{z^*}^{z_{\rm cut}} \right) \right] \frac{d\sigma}{dM\, dy\, dz} dz, \quad \text{if } z^* < z_{\rm cut}, \\
\frac{d\sigma_{\rm CE}}{dM} &= \frac{d\sigma}{dM}, \quad \text{if } z^* > z_{\rm cut},
\end{aligned} \tag{3.1}$$

where the $z_{\rm cut}$ is determined by detector capabilities, and $y_{\rm max}$ may be less than $Y = \log(\sqrt{s}/M)$ as a consequence of the angular cuts. When translated from the laboratory frame to the dilepton c.m. frame, the angular cuts become boost dependent. Hence, $z_{\rm cut} = z_{\rm cut}(y)$.

3.1 LHC

At the LHC, the lepton pseudorapidity cut is $|\eta| < \eta_{\rm cut} = 2.5$ for both leptons [25], which corresponds to $-z_{\rm cut}^{\rm lab} < z^{\rm lab} < z_{\rm cut}^{\rm lab}$ (with $z^{\rm lab} = \cos\theta_{\rm lab}$) and $z_{\rm cut}^{\rm lab} = \tanh\eta_{\rm cut} \simeq 0.987$. These cuts should however be transformed from the lab system to the c.m. system of the two leptons (where the leptons are back-to-back). This gives for the cosine of the lepton angles in the c.m. system the following 'visible' z range

$$\begin{aligned} -\tanh(\eta_{\rm cut}+y) <\quad & z < \tanh(\eta_{\rm cut}-y), \quad \text{for } l^-, \\ -\tanh(\eta_{\rm cut}+y) < & -z < \tanh(\eta_{\rm cut}-y), \quad \text{for } l^+, \end{aligned} \tag{3.2}$$

where y is the rapidity of the c.m. frame of the lepton pair w.r.t. the lab frame (pp c.m. frame). Note that for a given y the visible z region for detection of one lepton is not symmetric around $z = 0$ unless $y = 0$. Since we require *both* leptons to be detected, we combine the two regions given above into the symmetric region

$$|z| < \tanh(\eta_{\rm cut} - |y|) = \frac{z_{\rm cut}^{\rm lab} - |\beta|}{1 - z_{\rm cut}^{\rm lab}|\beta|} \equiv z_{\rm cut}, \tag{3.3}$$

where $\beta = \tanh y$. This means that we have to require $|y| < \eta_{\rm cut} = 2.5$ in addition to the limits $|y| < Y = \log(\sqrt{s}/M)$, hence $y_{\rm max} = \min(\eta_{\rm cut}, Y)$. At the LHC, the cut $|y| < \eta_{\rm cut}$ affects the rapidity integration range for values of M below 1.15 TeV.

In addition to the angular cuts, we impose on each lepton a transverse momentum cut

$$p_\perp > p_\perp^{\rm cut} = 20 \text{ GeV}, \tag{3.4}$$

which leads to $|z| < \sqrt{1 - (2p_\perp^{\rm cut}/M)^2}$. This cut affects the z integration range for $M < 0.25$ TeV at the LHC. Thus, the over-all cut on z will in general depend on both y and M.

3.2 Tevatron

At the Tevatron, the cuts are more complicated, since both detectors there have some additional coverage close to the beam pipe ('end plugs') in addition to the central part of the detector. As an example, we shall here consider the following cuts. We want either both leptons in the Central Calorimeter (CC), $|\eta| < 1.1$ (corresponding to $|z^{\rm lab}| < 0.800$) or one lepton in the Central Calorimeter and one lepton in an End Cap (EC), $1.5 < |\eta| < 2.5$ (corresponding to $0.905 < |z^{\rm lab}| < 0.987$) [26, 27] (see Fig. 4). We get the restrictions on the z range given in Appendix A, and shown in Fig. 5.

Since for rapidity y larger than 1.8 there is no integration range left, these cuts result in a rapidity cut in addition to the limit $|y| \leq \log(\sqrt{s}/M)$. This additional limitation, $|y| \leq 1.8$,

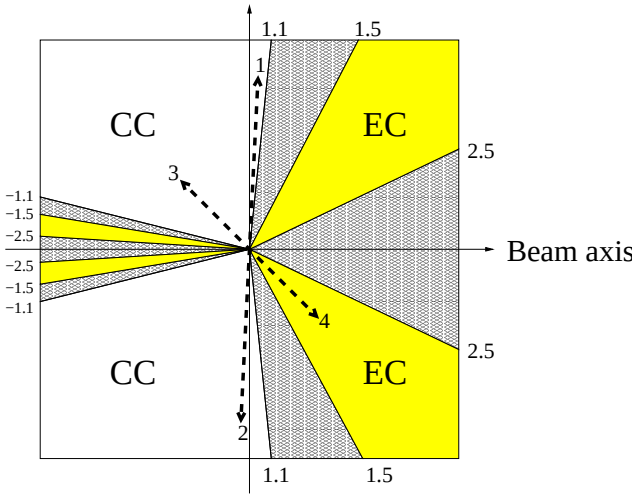

Figure 4: Schematic side view of Tevatron detector, as seen in the c.m. frame at a positive boost given by $y = 1.0$ ($\beta = 0.762$): Central Calorimeter (CC) and End Caps (EC) are indicated as white and yellow (shaded), with 'blind' directions dark. The borders between different regions are labeled by the corresponding pseudorapidity, $|\eta| = 1.1$, 1.5 or 2.5. The tracks labeled '1' and '2' are back-to-back in the CC, whereas '3' and '4' are back to back with '3' in the CC and '4' in the EC, compare Table 2 in Appendix A.

only affects the integration range in y for invariant dilepton masses $M < 0.32$ TeV at the Tevatron. Like for the LHC, we also impose the $p_\perp$ cut of Eq. (3.4).

Note that terms that are odd in $z = \cos\theta_{\rm cm}$ do not contribute to $A_{\rm CE}$, since, as previously emphasized, the integration limits are always symmetric around $z = 0$. Consequently, the applied experimental cuts in the laboratory frame must respect this symmetry in order to measure this observable.

3.3 The vanishing of $A_{\rm CE}^{\rm SM}$

As pointed out in the final part of Sec. 2.1, the zero point of $A_{\rm CE}$ can be a good indicator of the usefulness of this observable in discriminating against the SM as well as any new physics based on vector couplings. If the zero point is little changed by the inclusion of gravity effects, then it is unlikely that $A_{\rm CE}$ will be useful. We will now discuss approaches for obtaining $A_{\rm CE}^{\rm SM} = 0$ in the presence of angular cuts. This can be done either differentially in y, or after an integration over y.

3.3.1 A rapidity-dependent approach

One can define a value $\hat{z}_0^*$, such that the parton-level center–edge cross section vanishes:

$$\hat{\sigma}_{\rm CE}^{\rm SM}(z^* = \hat{z}_0^*) = 0. \tag{3.5}$$

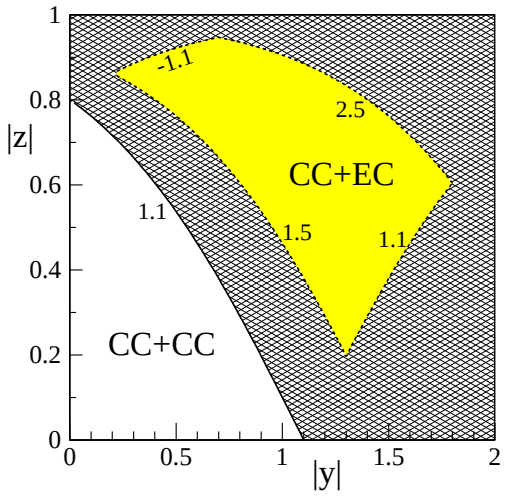

Figure 5: Cuts on $z = \cos\theta_{\rm cm}$ vs. c.m. rapidity y for the Tevatron. White: region allowed by having both leptons in the Central Calorimeter; yellow (shaded): region allowed by having one lepton in the Central Calorimeter and the other in an End Cap. Cuts are labeled by the corresponding pseudorapidities, compare Table 2 in Appendix A.

In the case of no angular cuts, $\hat{z}_0^* = z_0^*$, as given by Eq. (2.17). However, as anticipated at the beginning of this section, the introduction of cuts will contribute to a modification of this value, which will depend on both the rapidity and the invariant dilepton mass M considered.

When angular cuts are introduced ($|z| \leq z_{\rm cut}$), it follows from Eq. (2.15) that

$$\hat{\sigma}^{\rm SM}_{\rm CE}(z^*) \propto z^*(z^{*2}+3) - \tfrac{1}{2}\, z_{\rm cut}[z_{\rm cut}^2+3]. \tag{3.6}$$

One can thus determine the value of z^* for which $\hat{\sigma}^{\rm SM}_{\rm CE}$ vanishes, by solving a cubic equation. The solution can for the LHC be given by the simple expression

$$\hat{z}_0^* = (\sqrt{b}+a)^{1/3} - (\sqrt{b}-a)^{1/3}, \tag{3.7}$$

where

$$a = \tfrac{1}{4} z_{\rm cut}[z_{\rm cut}^2+3], \quad b = a^2+1, \tag{3.8}$$

generalizing Eq. (2.17). In Fig. 6, we display both $z_{\rm cut}$ and $\hat{z}_0^*$ as functions of y for two values of the invariant dilepton mass. Since $z_{\rm cut} = z_{\rm cut}(y)$ as given in Sec. 3.1, $\hat{z}_0^*$ will also depend on y, but not on M for $M > 0.25$ TeV, where the $p_\perp$ cut of Eq. (3.4) plays no role.

At the Tevatron, the corresponding cubic equation is more complicated, since there for some range of $|y|$ are two disjoint regions of $|z|$, and at large $|y|$, a region where low $|z|$ are disallowed (see Fig. 5).

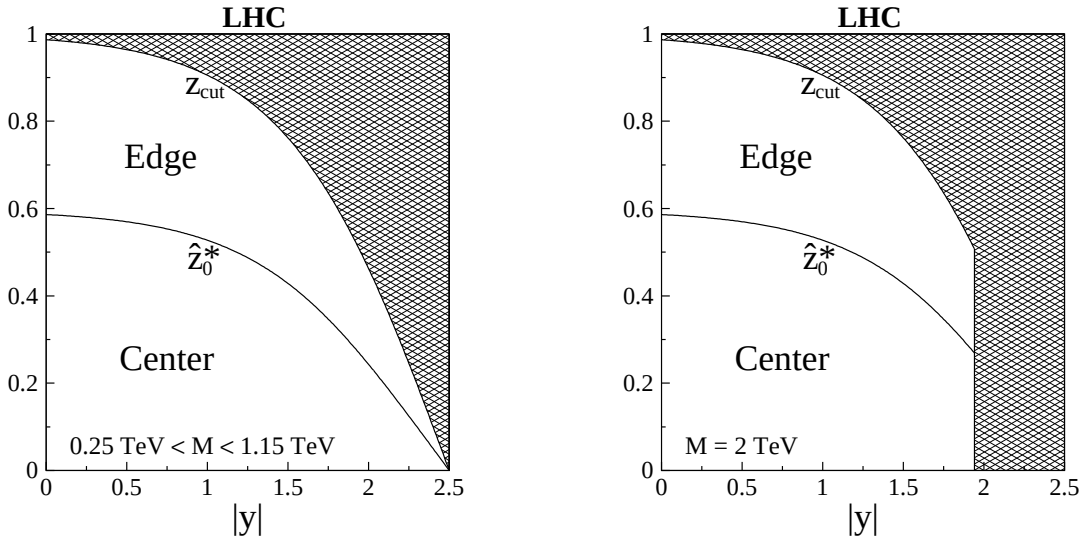

Figure 6: Dependence of $z_{\rm cut}$ and $\hat{z}_0^*$ on $|y|$ at the LHC for 0.25 TeV $< M <$ 1.15 TeV and $M = 2$ TeV. The dark regions are excluded by the cuts, the additional limitation on $|y|$ in the right-hand panel is due to the M-dependent kinematical limit $|y| \leq Y$.

3.3.2 Zeros of $A_{\rm CE}$ and their M dependence

It is also possible to make $A_{\rm CE}^{\rm SM}$ vanish after the introduction of cuts, by redefining z_0^* such that

$$\frac{d\sigma_{\rm CE}^{\rm SM}}{dM}(z^* = z_0^*) = 0. \tag{3.9}$$

This provides a more global value for z_0^*, but since the parton distribution functions are involved in the integration over y, we cannot find an analytic expression for this quantity.

With the cuts discussed in Secs. 3.1 and 3.2, and using the center–edge definition in Eq. (2.7), z_0^* depends on the invariant mass of the lepton-pair as shown in Fig 7 (the SM curve is the same in both panels). In addition to z_0^* (solid), we also plot the contours corresponding to $A_{\rm CE} = 0$ for $\lambda = \pm 1$ (dashed) in the z^*–M plane for two cases, $M_H = 2$ and 4 TeV, both at the LHC.

The M-dependence of z_0^* can qualitatively be understood as follows. At low invariant masses, also high y contribute to the cross section, but here z has an upper bound significantly below 1 (see Fig. 6). For higher masses, on the other hand, the dominant contribution comes from lower values of y, where z can reach higher values. In order to keep $d\sigma_{\rm CE}^{\rm SM}/dM = 0$, z_0^* has to increase with increasing mass M and tends to its asymptotic value ≈ 0.586, as seen in Fig. 7.

Let us next consider the difference between z_0^* for the SM and the z^* value at which $A_{\rm CE}$ vanishes for the ADD case. First of all, at low M, graviton exchange does not play any role, due to the strongly suppressing factors $(M/M_H)^4$ and $(M/M_H)^8$, see Eq. (2.15), so the SM and ADD curves coincide. At the LHC, where pure graviton exchange gives an

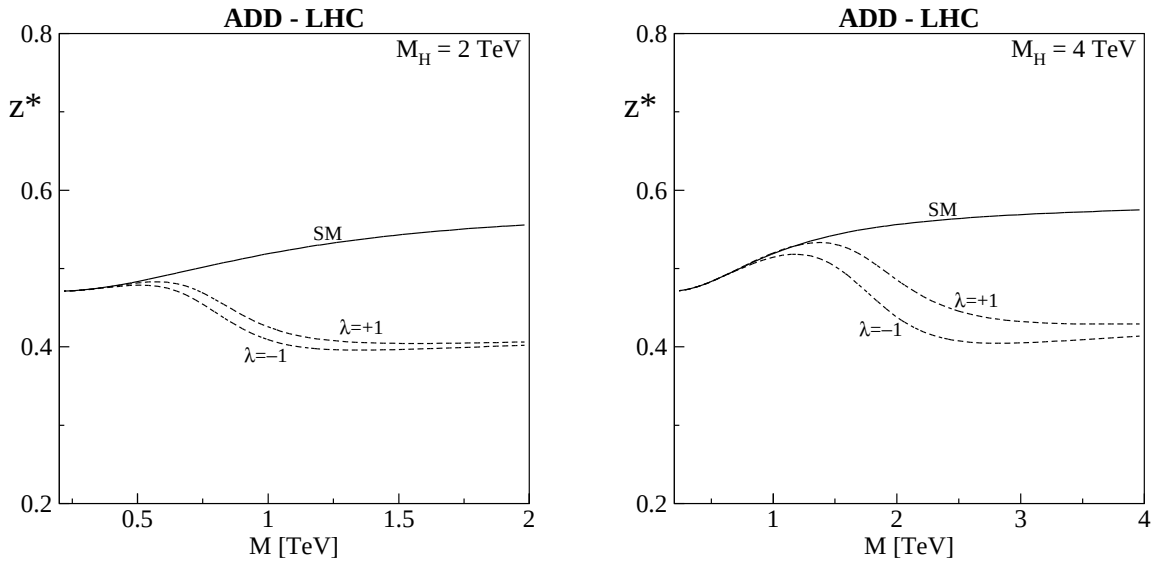

Figure 7: Zeros of $A_{\rm CE}$ and their M dependence at the LHC. The solid curves give z_0^*, which corresponds to $A_{\rm CE}^{\rm SM} = 0$, whereas the dashed curves correspond to $A_{\rm CE} = 0$ for the ADD model, with $M_H = 2$ and 4 TeV.

important contribution to $A_{\rm CE}$, z_0^* is larger, since pure graviton events are more central, as given by Eq. (2.21).

At the Tevatron, the more complicated cuts lead to a different behavior, with decreasing z_0^* as M increases. In addition, the values for z_0^* for the SM and the ADD model are rather close in the region where the majority of events will occur. Consequently, in the case of the Tevatron, the usefulness of $A_{\rm CE}$ is in fact not a priori guaranteed.

4 Identification of spin-2

In this section we assume that a deviation from the SM is discovered in the cross section, either in the form of a contact interaction or a resonance. We will here investigate in which regions of the ADD and RS parameter spaces such a deviation can be identified as being caused by spin-2 exchange. More precisely, we will see how the center–edge asymmetry can be used to exclude spin-1 exchange beyond that of the SM.

In order to get more statistics, one may integrate over bins i in M. We therefore define the bin-integrated center–edge asymmetry by introducing such an integration,

$$A_{\rm CE}(i) = \frac{\displaystyle\int_i \frac{d\sigma_{\rm CE}}{dM} dM}{\displaystyle\int_i \frac{d\sigma}{dM} dM}. \tag{4.1}$$

Here, the rapidity-dependent approach, with $\hat{z}_0^*(y)$ given by Eq. (3.7), and shown in Fig. 6 for the LHC, will be used. The advantage of this approach is that it is given by an explicit analytical expression, whereas the approach outlined in subsec. 3.3.2 depends on the M-range considered.

To determine the underlying new physics (spin-1 vs. spin-2 couplings) one can introduce the deviation of the measured center–edge asymmetry from that expected from pure spin-1 exchange, $A_{\rm CE}^{\text{spin-1}}(i)$ (which in our approach is zero), in each bin,

$$\Delta A_{\rm CE}(i) = A_{\rm CE}(i) - A_{\rm CE}^{\text{spin-1}}(i). \tag{4.2}$$

The bin-integrated statistical uncertainty is then given as

$$\delta A_{\rm CE}(i) = \sqrt{\frac{1 - A_{\rm CE}^2(i)}{\epsilon_l \mathcal{L}_{\rm int} \sigma(i)}}, \tag{4.3}$$

based on the number of events that are effectively detected and the $A_{\rm CE}$ that is actually measured. We take the efficiency for reconstruction of lepton pairs, $\epsilon_l = 90\%$ and sum over $l = e, \mu$.

The statistical significance, $\mathcal{S}_{\rm CE}(i)$ is defined as:

$$\mathcal{S}_{\rm CE}(i) = \frac{|\Delta A_{\rm CE}(i)|}{\delta A_{\rm CE}(i)}. \tag{4.4}$$

4.1 ADD case

In the ADD scenario, the identification reach in M_H can be estimated from a χ^2 analysis:

$$\chi^2 = \sum_i \left[\mathcal{S}_{\rm CE}(i)\right]^2, \tag{4.5}$$

where i runs over the different bins in M. The 95% CL is then obtained by requiring $\chi^2 = 3.84$, as pertinent to a one-parameter fit [28].

At the LHC, with 100 fb^{-1}, we require $M > 400$ GeV and divide the data into 200 GeV bins as long as the number of events in each bin, $\epsilon_l \mathcal{L}_{\rm int} \sigma(i)$, is larger than 10. Therefore, the number of bins will depend on the magnitude of the (discovered) deviation from the SM.

We find that at the 95% CL, the *identification* reach at the LHC, where one can distinguish between the ADD and an alternative spin-1 based scenario, is $M_H = 4.77$ TeV and 5.01 TeV for $\lambda = +1$ and -1, respectively. In the first case, we used 17 bins, whereas in the last case the number of bins was 13 (the numbers of bins are determined by the condition of having at least 10 events in each bin). If no cuts are imposed, one would obtain an improvement of the identification reach on M_H, by up to 2%, with $z_0^* \simeq 0.596$. Therefore, at the LHC, the cuts have only a moderate impact on the results.

At the Tevatron, with 2 fb^{-1}, the lower limit on M is chosen to be $M > 200$ GeV, with 50 GeV bins. We find for the identification reach, $M_H = 0.87$ TeV and 0.97 TeV for

$\lambda = +1$ and -1, with 13 and 8 bins, respectively. If no cuts are imposed, one would obtain slightly improved limits, namely $M_H = 0.99$ TeV and 1.06 TeV for the two cases, with 10 and 8 bins and $z_0^* \simeq 0.596$. Thus, the "modest" identification reach at the Tevatron is due to a combination of several effects (including partial cancellation of interference related to u and d quarks), and not primarily determined by the more severe cuts. However, these regions of parameter space have already been excluded by LEP [29] which has reached $M_H = 1.20$ and 1.09 TeV (for $\lambda = +1$ and -1) (for Fermilab results, see [30, 31]).

Table 1: Identification reach on M_H (in TeV) at 95% CL from $A_{\rm CE}$.

Collider	$\lambda = +1$	$\lambda = -1$
Tevatron 2 fb^{-1}	0.9	1.0
LHC 100 fb^{-1}	4.8	5.0
LHC 300 fb^{-1}	5.4	5.9

In Table 1 we summarize the results, and also include the identification reach corresponding to an integrated luminosity of 300 fb^{-1} at the LHC. The obtained results depend on the procedure adopted for the binning. Let us first discuss the case when we keep the range in M fixed, $M_{\rm min} \leq M \leq M_{\rm max}$, but increase the bin width. The identification reach turns out to be rather independent of the bin width, as long as it does not increase by more than a factor of order two, compared to the value we have adopted. The reason is that when the bins become too large, then contributions from low masses, where there are many (SM) events, will dilute the signal in $A_{\rm CE}$. On the other hand, if we make the bin width smaller, we would have to reduce $M_{\rm max}$, in order to satisfy the condition of having at least 10 events in the highest bin. Such a reduction of $M_{\rm max}$ normally leads to reduced sensitivity, since the new physics effects are strongest at high masses.

Consider next the case when we relax the constraint of keeping $M_{\rm max}$ fixed. Then, by increasing the chosen bin width, one could obtain a somewhat higher identification reach on M_H, since (in the approach we follow here) larger bin width would allow us to increase $M_{\rm max}$. However, keeping in mind the "effective character" of the interaction (2.11), such that M_H represents integration over masses up to a cut-off, one should be careful not to go too close to M_H.

In a less conservative approach, one could put all events between $M_{\rm max}$ and $0.9 \times M_H$ into one additional bin. If one were to do that, the identification reach would increase. For example, for the LHC case, with 100 fb^{-1} (see Table 1), the identification reach would increase by 4% and 13% for $\lambda = +1$ and -1, respectively.

4.2 RS case

A very distinct feature of the RS scenario is that the resonances are unevenly spaced. If the first resonance is sufficiently heavy, the second resonance would be difficult to resolve

within the kinematical range allowed experimentally. For $m_1 > 1.7$, 2.5, 2.8 TeV for $k/\bar{M}_{\rm Pl} = 0.01$, 0.05, 0.1, respectively, the second resonance would contain less than 10 events at the LHC, for 100 fb^{-1} (in the narrow-width approximation). The corresponding critical values at the Tevatron, for 2 fb^{-1}, are $m_1 > 0.28$, 0.44, 0.50 TeV. In this situation it would be of crucial importance to have a method of distinguishing between spin-1 and spin-2 resonances and, indeed, this is what the center–edge asymmetry can offer.

At the LHC (Tevatron), we choose a 200 GeV (50 GeV) bin around the resonance mass m_1, and obtain the results presented in Fig. 8, where we display the 2, 3 and 5σ contours, cf. Eq. (4.4), specialized to a single bin around m_1. In order not to create additional hierarchies, we require the scale of physical processes on the 'TeV brane', $\Lambda_\pi = m_1/[x_1(k/\bar{M}_{\rm Pl})] < 10$ TeV, as indicated in the figure [10]. Note that a spin-1 resonance (e.g., a Z') would give $\Delta A_{\rm CE} = 0$, provided we use $\hat{z}_0^*$ as given by Eq. (3.7), or its analogue for the Tevatron.

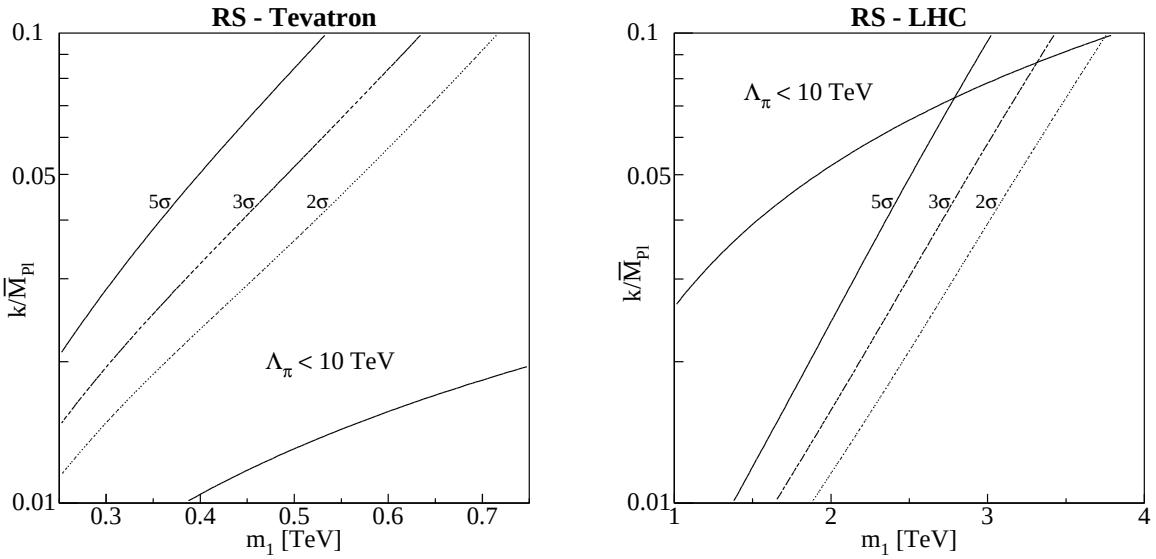

Figure 8: Spin-2 identification of an RS resonance, using the center–edge asymmetry. We integrate over bins of 50 and 200 GeV around the peak at the Tevatron and LHC, respectively. The theoretically favored region, $\Lambda_\pi < 10$ TeV, is indicated.

In the RS scenario, the LHC is capable of excluding or discovering graviton resonances [32] in the whole region referred to as the theoretically preferred part of the parameter space ($\Lambda_\pi < \mathcal{O}(10$ TeV$)$). We see that the center–edge asymmetry can distinguish spin-2 exchange from spin-1 exchange, in large parts of this theoretically favoured region. Note also that the corresponding bounds cover the regions of parameter space where only the first resonance is produced. The position of a second resonance would reveal its RS-nature from the mass splitting.

5 Concluding remarks

Exploring the center–edge asymmetry at hadron colliders is a good strategy to distinguish between spin-1 and spin-2 exchange. The proposed center-edge asymmetry may be seen as a possible alternative or supplement to a direct fit to the differential angular distribution [13, 32].

We have considered the ADD scenario parametrized by M_H, and the RS scenario parametrized by m_1 and $k/\bar{M}_{\rm Pl}$. Although somewhat higher sensitivity reaches on M_H or m_1 than obtained here are given by other approaches, this method based on $A_{\rm CE}$ is suitable for actually pinning down the spin-2 nature of the KK gravitons up to very high M_H or m_1. This is different from just detecting deviations from the Standard Model predictions, and is a way to obtain additional information on the underlying new-physics scenario.

The results obtained appear to be only moderately dependent on the parametrization of the parton distribution functions used. Compared to CTEQ6 [24], the MRST parametrization [33], gives practically no change in $A_{\rm CE}$ (since this is obtained as a ratio), but changes the identification reach by 1-2%, since the cross section increases and therefore the statistics improve.

The *identification* of a spin-2 exchange relies on first discovering a deviation from the Standard Model. For this purpose, the conventional cross section, σ, is more sensitive than $A_{\rm CE}$. The sensitivity of σ can be further extended by considering also the forward–backward asymmetry, $A_{\rm FB}$, especially at the Tevatron, where the $q\bar{q}$ channel is important. At the LHC, $A_{\rm FB}$ is less useful, since it is insensitive to the gluon–gluon channel, as already remarked in Sec. 2, and since a cut of $|y| > 1$ is needed to enhance the probability to experimentally identify the proton from which the quark originated, thus reducing the number of events.

At a hadron collider, the case of spin-0 exchange would be more difficult to discriminate against, since the difference in $A_{\rm CE}$ would be smaller. However, at an electron-positron collider with polarized beams, there are more observables available, and hence a discrimination might be possible [7, 11].

We have here considered the dilepton channels. The identification reach can of course be extended by the inclusion of the diphoton and possibly also the dijet channels.

Acknowledgment
We are grateful to Tom Rizzo for useful communication. One of us (AAP) wants to express his gratitude to N. Rusakovich and N. Shumeiko for stimulating discussions. This research has been partially supported by MIUR (Italian Ministry of University and Research), by funds of the University of Trieste, and by the Research Council of Norway.

Appendix A

In order to provide a compact description of the integration ranges of z that are involved for various values of the rapidity y, let us introduce the abbreviation

$$z_{\rm cut}(\eta_i, y) = \tanh(\eta_i - |y|). \tag{A1}$$

According to Sec. 3.2, we determine the cuts in z, for $\eta_1 = 1.1$, $\eta_2 = 1.5$ and $\eta_3 = 2.5$. Leptons are either both in the Central Calorimeter, $|\eta| < 1.1$ ("CC & CC") or one lepton is in the Central Calorimeter and one is in the End Cap, $1.5 < |\eta| < 2.5$ ("CC & EC"). The resulting limits are summarized in Table 2.

Table 2: Tevatron cuts on the c.m. angle, in terms of $|z|$.

c.m. rapidity y	CC & CC	CC & EC
$0 \le \|y\| \le 0.2$	$\|z\| \le z_{\rm cut}(1.1, y)$	
$0.2 \le \|y\| \le 0.7$	$\|z\| \le z_{\rm cut}(1.1, y)$	$z_{\rm cut}(1.5, y) \le \|z\| \le \|z_{\rm cut}(-1.1, y)\|$
$0.7 \le \|y\| \le 1.1$	$\|z\| \le z_{\rm cut}(1.1, y)$	$z_{\rm cut}(1.5, y) \le \|z\| \le z_{\rm cut}(2.5, y)$
$1.1 \le \|y\| \le 1.3$		$z_{\rm cut}(1.5, y) \le \|z\| \le z_{\rm cut}(2.5, y)$
$1.3 \le \|y\| \le 1.8$		$\|z_{\rm cut}(1.1, y)\| \le \|z\| \le z_{\rm cut}(2.5, y)$

At low rapidities, there is only one range in z (where both leptons hit the CC), whereas for intermediate rapidities y there are three ranges: for 'small' $|z|$ both leptons hit the CC, whereas at 'larger' values of $|z|$ (z being positive or negative) one lepton hits the CC and the other hits an EC (a representative case, with $y = 1$, is illustrated by Fig. 4). Finally, at 'large' rapidities, there are only two ranges of positive or negative values of z for which one lepton hits the CC and the other hits an EC. For rapidities above 1.8, there is no z range left.

References

[1] G. 't Hooft, in "Recent Developments In Gauge Theories", Proceedings, NATO Advanced Study Institute, Cargese, France, August 26 - September 8, 1979, edited by G. 't Hooft, C. Itzykson, A. Jaffe, H. Lehmann, P. K. Mitter, I. M. Singer and R. Stora *New York, USA: Plenum (1980) (NATO Advanced Study Institutes Series: Series B, Physics, 59)*;
S. Dimopoulos, S. Raby and L. Susskind, Nucl. Phys. B **173** (1980) 208.

[2] E. Eichten, K. D. Lane and M. E. Peskin, Phys. Rev. Lett. **50** (1983) 811;
R. Ruckl, Phys. Lett. B **129** (1983) 363.

[3] V. D. Barger, K. m. Cheung, K. Hagiwara and D. Zeppenfeld, Phys. Rev. D **57** (1998) 391 [arXiv:hep-ph/9707412];

D. Zeppenfeld and K. m. Cheung, Proceedings of 5th International WEIN Symposium: A Conference on Physics Beyond the Standard Model (WEIN 98), Santa Fe, NM, 14–21 Jun 1998; arXiv:hep-ph/9810277.

[4] For reviews see, *e.g.*: J. L. Hewett and T. G. Rizzo, Phys. Rept. **183** (1989) 193;
A. Leike, Phys. Rept. **317** (1999) 143 [arXiv:hep-ph/9805494];

[5] W. Buchmuller, R. Ruckl and D. Wyler, Phys. Lett. B **191** (1987) 442 [Erratum-ibid. B **448** (1999) 320];
G. Altarelli, J. R. Ellis, G. F. Giudice, S. Lola and M. L. Mangano, Nucl. Phys. B **506** (1997) 3 [arXiv:hep-ph/9703276];
R. Casalbuoni, S. De Curtis, D. Dominici and R. Gatto, Phys. Lett. B **460** (1999) 135 [arXiv:hep-ph/9905568];
V. D. Barger and K. m. Cheung, Phys. Lett. B **480** (2000) 149 [arXiv:hep-ph/0002259].

[6] J. Kalinowski, R. Ruckl, H. Spiesberger and P. M. Zerwas, Phys. Lett. B **406** (1997) 314 [arXiv:hep-ph/9703436]; Phys. Lett. B **414** (1997) 297 [arXiv:hep-ph/9708272].

[7] T. G. Rizzo, Phys. Rev. D **59** (1999) 113004 [arXiv:hep-ph/9811440].

[8] G. J. Gounaris, D. T. Papadamou and F. M. Renard, Phys. Rev. D **56** (1997) 3970 [arXiv:hep-ph/9703281].

[9] J. L. Hewett, Phys. Rev. Lett. **82** (1999) 4765 [arXiv:hep-ph/9811356].

[10] H. Davoudiasl, J. L. Hewett and T. G. Rizzo, Phys. Rev. Lett. **84** (2000) 2080 [arXiv:hep-ph/9909255];
H. Davoudiasl, J. L. Hewett and T. G. Rizzo, Phys. Rev. D **63** (2001) 075004 [arXiv:hep-ph/0006041].

[11] P. Osland, A. A. Pankov and N. Paver, Phys. Rev. D **68**, 015007 (2003) [arXiv:hep-ph/0304123].

[12] I. Antoniadis, N. Arkani-Hamed, S. Dimopoulos and G. R. Dvali, Phys. Lett. B **436** (1998) 257 [arXiv:hep-ph/9804398];
N. Arkani-Hamed, S. Dimopoulos and G. R. Dvali, Phys. Rev. D **59** (1999) 086004 [arXiv:hep-ph/9807344];
G. F. Giudice, R. Rattazzi and J. D. Wells, Nucl. Phys. B **544** (1999) 3 [arXiv:hep-ph/9811291]; Nucl. Phys. B **630** (2002) 293 [arXiv:hep-ph/0112161];
E. A. Mirabelli, M. Perelstein and M. E. Peskin, Phys. Rev. Lett. **82** (1999) 2236 [arXiv:hep-ph/9811337];
T. Han, J. D. Lykken and R. J. Zhang, Phys. Rev. D **59** (1999) 105006 [arXiv:hep-ph/9811350];
K. m. Cheung, Phys. Rev. D **61**, 015005 (2000) [arXiv:hep-ph/9904266];
L. Randall and R. Sundrum, Phys. Rev. Lett. **83** (1999) 4690 [arXiv:hep-th/9906064];
S. Cullen, M. Perelstein and M. E. Peskin, Phys. Rev. D **62** (2000) 055012

[arXiv:hep-ph/0001166];
J. Bijnens, P. Eerola, M. Maul, A. Månsson and T. Sjöstrand, Phys. Lett. B **503** (2001) 341 [arXiv:hep-ph/0101316];
T. G. Rizzo, Phys. Rev. D **64** (2001) 095010 [arXiv:hep-ph/0106336];
K. m. Cheung and G. Landsberg, Phys. Rev. D **65** (2002) 076003 [arXiv:hep-ph/0110346];
G. Pasztor and M. Perelstein, in *Proc. of the APS/DPF/DPB Summer Study on the Future of Particle Physics (Snowmass 2001)* ed. N. Graf, arXiv:hep-ph/0111471;
E. Gabrielli and B. Mele, Nucl. Phys. B **647**, 319 (2002) [arXiv:hep-ph/0205099];
E. Dvergsnes, P. Osland and N. Öztürk, Phys. Rev. D **67**, 074003 (2003) [arXiv:hep-ph/0207221].

[13] B. C. Allanach, K. Odagiri, M. A. Parker and B. R. Webber, JHEP **0009**, 019 (2000) [arXiv:hep-ph/0006114].

[14] N. Arkani-Hamed, S. Dimopoulos and G. R. Dvali, Phys. Lett. B **429** (1998) 263 [arXiv:hep-ph/9803315].

[15] L. Randall and R. Sundrum, Phys. Rev. Lett. **83** (1999) 3370 [arXiv:hep-ph/9905221].

[16] K. R. Dienes, E. Dudas and T. Gherghetta, Phys. Lett. B **436**, 55 (1998) [arXiv:hep-ph/9803466].

[17] V. A. Rubakov and M. E. Shaposhnikov, Phys. Lett. B **125** (1983) 136.

[18] I. Antoniadis, Phys. Lett. B **246** (1990) 377;
I. Antoniadis and K. Benakli, Phys. Lett. B **326**, 69 (1994) [arXiv:hep-th/9310151];
I. Antoniadis, K. Benakli and M. Quiros, Phys. Lett. B **331**, 313 (1994) [arXiv:hep-ph/9403290].

[19] A. A. Pankov, N. Paver and C. Verzegnassi, Int. J. Mod. Phys. A **13**, 1629 (1998) [arXiv:hep-ph/9701359].

[20] J. Hewett and M. Spiropulu, Ann. Rev. Nucl. Part. Sci. **52**, 397 (2002) [arXiv:hep-ph/0205106].

[21] G. F. Giudice and A. Strumia, Nucl. Phys. B **663**, 377 (2003) [arXiv:hep-ph/0301232].

[22] A. K. Gupta, N. K. Mondal and S. Raychaudhuri, arXiv:hep-ph/9904234;
K. m. Cheung and G. Landsberg, Phys. Rev. D **62**, 076003 (2000) [arXiv:hep-ph/9909218].

[23] A. Datta, E. Gabrielli and B. Mele, Phys. Lett. B **552**, 237 (2003) [arXiv:hep-ph/0210318].

[24] J. Pumplin, D. R. Stump, J. Huston, H. L. Lai, P. Nadolsky and W. K. Tung, JHEP **0207** (2002) 012 [arXiv:hep-ph/0201195].

[25] A. Airapetian *et al.*, *ATLAS detector and Physical Performance Technical Design Report,*
http://atlasinfo.cern.ch/Atlas/GROUPS/PHYSICS/TDR/access.html,
G. L. Bayatian *et al.*, *CMS Technical Proposal*, CERN LHCC 94-38 (1994),
http://cmsinfo.cern.ch/TP/TP.html.

[26] S. Abachi [The D0 Collaboration], *The D0 upgrade: The detector and its physics*, FERMILAB-PUB-96-357-E,
http://library.fnal.gov/archive/test-preprint/fermilab-pub-96-357-e.shtml,
R. Blair et al [The CDF Collaboration] *The CDF II Detector, Technical Design Report*, FERMILAB-Pub-96/390-E,
http://www-cdf.fnal.gov/upgrades/tdr/tdr.html

[27] M. P. Giordani [CDF and D0 Collaborations], FERMILAB-CONF-03-348-E *Presented at International Europhysics Conference on High-Energy Physics (HEP 2003), Aachen, Germany, 17-23 Jul 2003*;
L. Cerrito [the CDF Collaboration], arXiv:hep-ex/0311050;
[CDF Collaboration], arXiv:hep-ex/0311039.

[28] W. T. Eadie, D. Drijard, F. E. James, M. Roos, B. Sadoulet, *Statistical methods in experimental physics* (American Elsevier, 1971).

[29] LEPEWWG $f\bar{f}$ SubGroup (C. Geweniger *et. al.*), Combination of the LEP II $f\bar{f}$ Results, CERN preprint LEP2FF/02-03 (October 2002).

[30] B. Abbott *et al.* [D0 Collaboration], Phys. Rev. Lett. **86**, 1156 (2001) [arXiv:hep-ex/0008065].

[31] M. Sanders [CDF Collaboration], arXiv:hep-ex/0310033.

[32] P. Traczyk and G. Wrochna, arXiv:hep-ex/0207061;
C. Collard, M.-C. Lemaire, P. Traczyk, G. Wrochna, CMS NOTE-2002/050

[33] A. D. Martin, R. G. Roberts, W. J. Stirling and R. S. Thorne, Phys. Lett. B **443**, 301 (1998) [arXiv:hep-ph/9808371]; arXiv:hep-ph/0307262.